

CO₂ Activation by metal–ligand-cooperation mediated by iridium pincer complexes

Moran Feller, Eyal Ben-Ari, Yael Diskin-Posner & David Milstein

To cite this article: Moran Feller, Eyal Ben-Ari, Yael Diskin-Posner & David Milstein (2018): CO₂ Activation by metal–ligand-cooperation mediated by iridium pincer complexes, Journal of Coordination Chemistry, DOI: [10.1080/00958972.2018.1475662](https://doi.org/10.1080/00958972.2018.1475662)

To link to this article: <https://doi.org/10.1080/00958972.2018.1475662>

 View supplementary material 

 Accepted author version posted online: 11 May 2018.

 Submit your article to this journal 

 Article views: 2

 View related articles 

 View Crossmark data 

Publisher: Taylor & Francis

Journal: *Journal of Coordination Chemistry*

DOI: <http://doi.org/10.1080/00958972.2018.1475662>



CO₂ Activation by metal–ligand-cooperation mediated by iridium pincer complexes

MORAN FELLER*[†], EYAL BEN-ARI[†], YAEL DISKIN-POSNER[‡] and DAVID MILSTEIN*[†]

Departments of [†]Organic Chemistry and [‡]Chemical Research Support, Weizmann Institute of Science, Rehovot 76100, Israel

Herein we report the reversible activation of CO₂ by the dearomatized complex [(^tBuPNP*)Ir(COE)] (**1**) and by the aromatized complex [(^tBuPNP)Ir(C₆H₅)] (**2**) via metal-ligand cooperation (MLC) (^tBuPNP = 2,6-bis-(di-tert-butylphosphinomethyl)pyridine; ^tBuPNP* = deprotonated PNP; COE = cyclooctadiene). The [1,3]-addition of CO₂ to **1** and **2** is reversible at ambient temperature. While the dearomatized complex **1** reacts readily at ambient temperature with CO₂ in THF or benzene, complex **2** reacts with CO₂ upon heating in benzene at 80 °C or at ambient temperature in THF. The novel aromatized complex [(^tBuPNP)IrCl] (**10**) does not react with CO₂. Based on the reactivity patterns of **1**, **2** and **10** with CO₂, we suggest that CO₂ activation via MLC takes place only via the dearomatized species, and that in the case of **2** THF plays a role as a polar solvent in facilitating formation of the dearomatized hydrido phenyl complex intermediate (complex **II**).

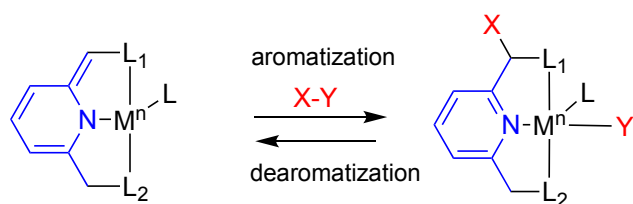
Keywords: Iridium complex; Carbon dioxide, CO₂ Activation; Metal-ligand cooperation

1. Introduction

In recent years our group has developed a new mode of metal–ligand cooperation (MLC) involving aromatization/dearomatization of lutidine-based pincer complexes (scheme 1) [1-6]. This new mode of reactivity enables the activation of various substrates such as alcohols [7-11], amines [12-15], nitriles [16, 17], boranes [18], dihydrogen [19-21], as well as activation of Csp²–H [22], and Csp³–H [23] bonds.

*Corresponding authors. Email: moran.feller@weizmann.ac.il (M. Feller); david.milstein@weizmann.ac.il (D. Milstein)

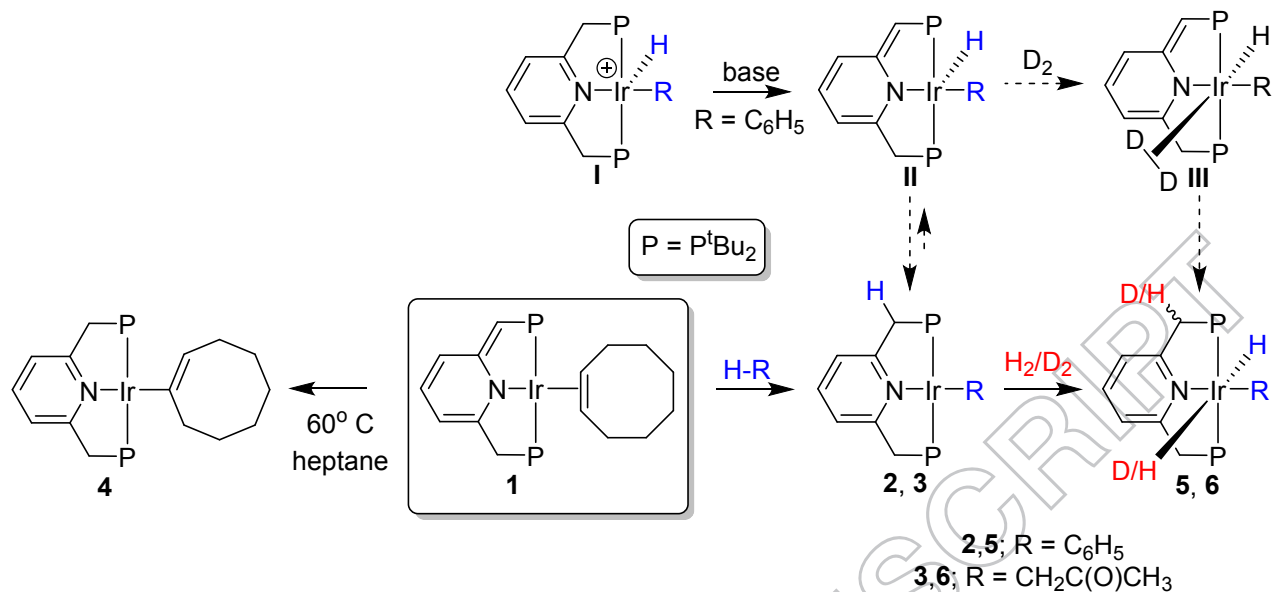
[†]Present address: Ph.D. R&D Team Leader, Agan Aroma & Fine Chemicals Ltd.



Scheme 1. Activation of chemical bonds (X-Y) by aromatization-dearomatization MLC with no change in the metal oxidation state.

This novel mode of bond activation by MLC is a key step in environmentally benign catalysis [1-5], allowing C–C bond formation between the exo-cyclic methine carbon of dearomatized pincer complexes and CO₂ [24-28] carbonyl compounds [29] and nitriles [30].

The dearomatized [(^tBuPNP*)Ir(COE)] (**1**) (^tBuPNP* = deprotonated ^tBuPNP ligand, COE = cyclooctene) was reported by us to activate both Csp²–H [22] and Csp³–H [23] bonds. Thus, reaction of **1** with benzene or acetone yielded the aromatized phenyl or acetonyl complexes **2** and **3**, respectively. Intramolecular Csp²–H activation via MLC also took place when **1** was heated in heptane, yielding the aromatized vinyl complex [(^tBuPNP)Ir(C₈H₁₃)] (**4**) (scheme 2). Complexes **2** and **3** also activate H₂ by MLC to give the *trans* dihydride phenyl- and acetonyl- complexes **5** and **6**, respectively. Upon reaction with D₂ the *trans* hydride-deuteride complexes [(^tBuPNP)Ir(H)(D)(R)], bearing one deuterium incorporated into a benzylic position, are obtained (scheme 2) [22, 23].



Scheme 2. Csp²-H, Csp³-H, and H₂ activation by ^tBuPNP-Ir complexes via MLC.

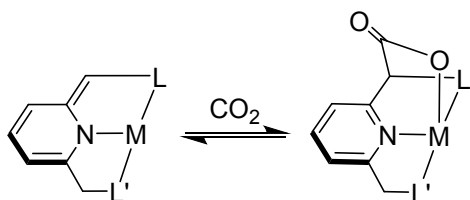
Intermediate **II** was observed upon deprotonation of complex **I**.

DFT calculations indicate that the active complexes in the H₂ activation process are actually Ir^{III} dearomatized intermediates [(^tBuPNP*)Ir(H)(R)] (**II**, scheme 2), which are in equilibrium with the aromatic Ir^I complexes [(^tBuPNP)Ir(R)] (**1** and **2**) [23, 31]. Although such equilibria were not directly observed, complex **II** (R = C₆H₅) was observed as the kinetic product upon deprotonation of the cationic complex [(^tBuPNP)Ir(H)(C₆H₅)] [BF₄] (**I**) at -78 °C and was trapped by CO to give the dearomatized complex [(^tBuPNP*)Ir(CO)(H)(C₆H₅)] [22].

Complexes **2** and **3** also activate O₂ via MLC to give the dearomatized complexes [(^tBuPNP*)Ir(H)(OH)(R)] (R = C₆H₅, CH₂C(O)CH₃) [32]. [(^tBuPNP*)Ir(H)(OH)(C₆H₅)] exhibits interesting reactivity with CO₂, giving an aromatized carbonate complex via MLC from a bicarbonate intermediate [32].

The reactivity of CO₂ with transition metal complexes is of interest and was explored intensively as it may lead to catalytic utilization of CO₂ as a C1 building block for the chemical industry [33-36]. CO₂ binding to metal centers can involve metal-carbon σ bonding (η¹-C) or metal-oxygen bonding (η¹-O, η²-O,O) and π bonding (η²-CO) [37]. CO₂ can also serve as a bridging ligand, forming polymetallic complexes [38]. Our group [25] and the group of Sanford [26] demonstrated a unique CO₂ activation mode by dearomatized pincer complexes via metal-

ligand cooperation (MLC). A concerted [1,3]-addition of CO₂ to the exo-cyclic carbon of a dearomatized pincer ligand takes place, resulting in the formation of new C–C and M–O bonds (scheme 3). This mode of CO₂ activation by MLC was reported to take place reversibly by ^tBuPNP Ru and Re complexes as well as by a PNN Ru complex (PNN = 2-(CH₂-P^tBu₂)-6-(CH₂-NEt₂)C₅H₃N) [24, 26, 28].



Scheme 3. Reversible CO₂ activation by PNP and PNN late transition complexes via MLC.

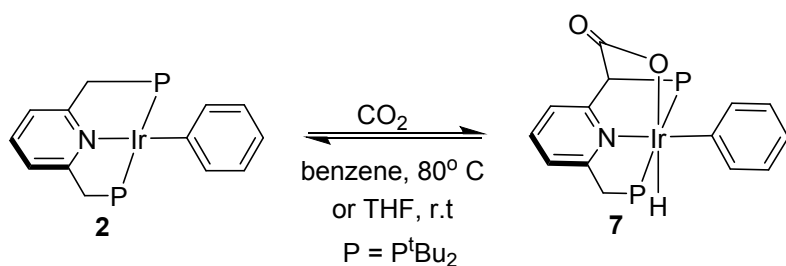
Recently we reported on CO₂ cleavage by a mixture of two complexes, [(^tBuPNP)IrH] and [(^tBuPNP*)Ir(H)₂], to give water and the dearomatized carbonyl complex [(^tBuPNP*)Ir(CO)] as a thermodynamic product. Exploring the reaction mechanism, we were able to identify [(^tBuPNP-COO)Ir(H)₂] as a kinetic product [27].

Herein we report the activation of CO₂ via MLC by the dearomatized complex [(^tBuPNP*)Ir(COE)] (**1**) and by [(^tBuPNP)Ir(C₆H₅)] (**2**).

2. Results and discussion

CO₂ reacts instantly with **2** at ambient temperature in THF (scheme 4). Upon addition of about 3 equiv of CO₂ to a THF solution of **2**, the [1,3]-addition product [(^tBuPNP-COO)Ir(C₆H₅)(H)] (**7**) was observed by NMR spectroscopy. Complex **7** exhibits an AB signal in the ³¹P{¹H} NMR (δ_P: 56.75 and 69.55 ppm, ²J_{PP} = 356.3 Hz), indicating two non-equivalent P-atoms. The ¹H NMR of **7** exhibits a hydride signal which appears as a doublet of doublets at -24.07 (²J_{PP} = 18.8, 7.5 Hz). The CO₂ carbon gives rise to a doublet of doublets signal at 171.34 ppm (²J_{PC} = 7.8 Hz, ⁵J_{PC} = 2.2 Hz) and an IR band at 1640 cm⁻¹. The benzylic proton adjacent to the bound CO₂ (Py-CH-COO) gives a long range correlation (²J) with the CO₂ carbon in the 2D-HMBC NMR spectrum. The phenyl ring gives five distinguishable signals, indicating a rigid structure with no free rotation of the phenyl ring.

The reaction of **2** with CO₂ is highly solvent dependent. While the reaction in THF was instantaneous at ambient temperature, under similar conditions in benzene, a mixture of unidentified products including the starting complex **2** was obtained according to ³¹P{¹H} NMR of the reaction mixture (see Supporting Information). Surprisingly, addition of CO₂ to a benzene solution of **2** preheated to 80 °C resulted in full conversion to **7**.



Scheme 4. Reaction of **2** with CO₂ to give the aromatized [1,3]-addition product **7**.

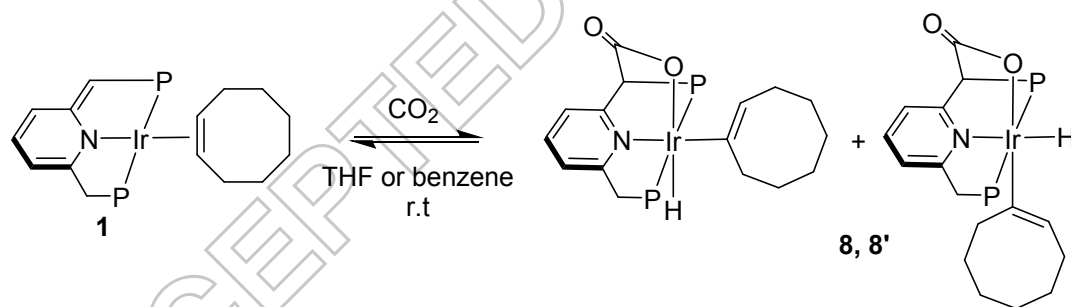
Complex **1** also reacts with CO₂. Upon reaction of **1** with 1 equiv of CO₂ at ambient temperature a mixture containing two major complexes was obtained (**8** and **8'**, scheme 5). We have assigned these complexes as the isomers which can be obtained upon [1,3]-addition of CO₂ to **1**, with the hydride located *trans* to the oxygen of the activated CO₂, or *trans* to the pyridine moiety of the PNP ligand, based on NMR spectroscopy (scheme 5).

The ³¹P{¹H} NMR spectrum of the reaction mixture gives overlapped AB signals in the region of 50 – 60 ppm. The ¹H NMR spectrum exhibits two hydride signals as a doublet of doublets (δH : -25.16 ($^2J_{\text{PH}} = 6.7, 18.6$ Hz) and -24.98 ($^2J_{\text{PH}} = 7.4, 19.3$ Hz) and in the ¹³C{¹H} NMR spectrum two doublet of doublets signals at 171.44 ($J_{\text{PC}} = 2.2, 7.0$ Hz) and 171.86 ppm (dd, $J_{\text{PC}} = 2.3, 8.2$ Hz) were assigned to the CO₂ carbons, as confirmed by using ¹³CO₂. 2D NMR experiments allowed us to assign the hydride signals with their corresponding signals in the ³¹P NMR, and $^3J_{\text{CH}}$ correlations between the hydrides and the corresponding CO₂ carbons was observed in the HMBC spectrum (figure 1). The benzylic protons of **8** and **8'** adjacent to the bound CO₂ give doublet of doublets signals at 4.99 ($J_{\text{PH}} = 2.2, 6.4$ Hz) and 4.92 ($J_{\text{PH}} = 1.4, 5.4$ Hz) ppm. When ¹³CO₂ was used, these signals appeared as multiplets due to ¹³C-H coupling, with a value of $^2J_{\text{CH}} = 3.9$ and 4.1 Hz, assigned by ¹H{³¹P} NMR.

When the reaction mixture was left in an NMR tube for 4 days single crystals suitable for X-ray diffraction were obtained, revealing an aromatized carbonate complex (**9**, figure 2), which was probably obtained by protonation of **8** with traces of water in the reaction mixture.

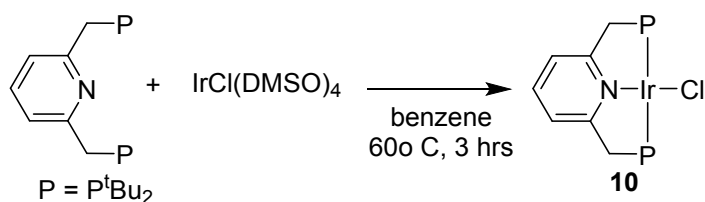
Complexes **7**, **8** and **8'** exhibit reversible binding of CO₂. According to ³¹P{¹H} NMR, about 20% and 30% conversion of complex **7** to **2** took place under vacuum after 2 and 5 h, respectively. Similar conversion was observed with **8** and **8'** to give **1** (see Supporting Information). Moreover, addition of ¹³CO₂ to THF solutions of **7** or **8** and **8'** afforded the labeled complexes **7**-¹³CO₂, **8**-¹³CO₂ and **8'**-¹³CO₂ as observed by NMR. In contrast to similar complexes which we have reported in the past to reversibly activate CO₂ such as [(^tBuPNP-COO)Ir(H)₂] [27] and [(^tBuPNP-COO)Ru(H)(CO)] [24] which lose the bound CO₂ readily at ambient temperature or under vacuum, **7**, **8** and **8'** exhibit greater stability, similar to the recently reported [(^tBuPNP-COO)Re(CO)₂] complex [28].

Unlike the reaction of **2** with CO₂, which is highly solvent dependent, the reaction of **1** with CO₂ takes place at ambient temperature in both THF and benzene. While **2** reacts with one equiv or excess of CO₂ to give **7**, addition of a large excess of CO₂ to **1** in benzene yielded a white precipitate, which is stable only under CO₂ atmosphere. Upon CO₂ removal, **1** was regenerated.



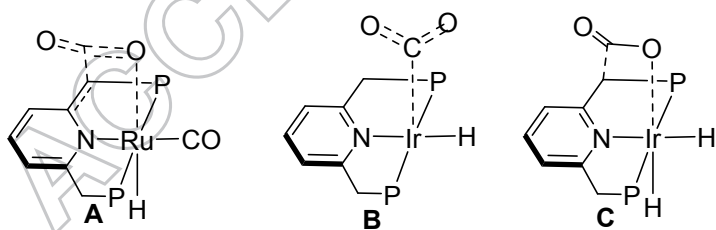
Scheme 5. Reaction of **1** with CO₂ to give the aromatized [1,3]-addition isomers **8** and **8'**.

The Ir^I complex [(^tBuPNP)IrCl] (**10**) was prepared as described in scheme 6. The ³¹P{¹H} NMR spectrum of **10** exhibits a sharp singlet, and the CH₂-P benzylic protons exhibit in the ¹H NMR spectrum only one virtual triplet signal, as expected for a square planar complex. The same geometry was also found in the solid state of **10** (figure 3). Unlike **1** and **2**, complex **10** was inert under CO₂ atmosphere (1 bar).



Scheme 6. Synthesis of **10**.

As mentioned above, while **1** reacts readily with CO_2 at ambient temperature in benzene or THF, complex **2** reacts with CO_2 in benzene only at 80°C , and at ambient temperature in THF. As we previously reported [24], DFT calculations regarding the reaction of $[(^t\text{BuPNP}^*)\text{Ru}(\text{H})(\text{CO})]$ with CO_2 to give $[(^t\text{BuPNP-COO})\text{Ru}(\text{H})(\text{CO})]$ showed that the most likely reaction pathway is [1,3]-addition, which proceeds without prior coordination of CO_2 to the metal center. The suggested transition state (**A**, scheme 7) provided a reaction barrier of $\Delta G^\ddagger_{298\text{K}} = 15.4 \text{ mol}^{-1}$, which is in line with the experimental value obtained from VT SST NMR measurements ($\Delta G^\ddagger_{298\text{K}} = 20.7 \pm 0.9 \text{ mol}^{-1}$). In addition, DFT calculations performed on the reaction pathway of $[(^t\text{BuPNP}^*)\text{Ir}(\text{H})_2]$ and $[(^t\text{BuPNP})\text{IrH}]$ with CO_2 support a [1,3]-addition of CO_2 to the dearomatized complex $[(^t\text{BuPNP}^*)\text{Ir}(\text{H})_2]$, which does not take place with the aromatized complex $[(^t\text{BuPNP})\text{IrH}]$ [27]. Thus, the calculated HOMO orbital of $[(^t\text{BuPNP})\text{IrH}]$ exhibits a d_{z^2} orbital on the Ir^I center, in line with a nucleophilic attack of Ir^I on CO_2 to give transition state **B** (scheme 7). The HOMO representation of $[(^t\text{BuPNP}^*)\text{Ir}(\text{H})_2]$ exhibits the highest coefficient at the deprotonated benzylic position, in line with the observed [1,3]-addition of CO_2 to transition state **C** [27].



Scheme 7. DFT optimized structures of the transition states for the reactions of PNP Ru and Ir complexes with CO_2 .

From the above mentioned DFT calculations we conclude that [1,3]-addition of CO₂ takes place only with dearomatized complexes. This is in line with our experimental findings which demonstrated facile CO₂ addition by the dearomatized **1** in benzene while the aromatized complex **10** did not react with CO₂. Regarding the reactivity of the aromatized **2** with CO₂, we believe that the actual active complex is a dearomatized Ir^{III} hydrido phenyl complex (**II**, scheme 1). As mentioned previously, experimental data and DFT calculations support an equilibrium between complexes **II** and **2**. Although it was calculated to have a non-realistic barrier of $\Delta G^\ddagger = 35.9 \text{ kcal mol}^{-1}$, if two water molecules are added to the transition state for “proton-transfer” assistance, then the transition state is substantially lowered in energy to $\Delta G^\ddagger = 20.7 \text{ kcal mol}^{-1}$. Thus, this process is catalyzed by adventitious water. However, such an equilibrium between **II** and **2** was not directly observed. Complex **II** was identified as the kinetic product of the deprotonation of **I** by low-temperature NMR experiment, leading to the exclusive formation of **2** as the thermodynamic product at ambient temperature. We believe that in benzene solution heating is required due to a higher activation barrier for the transformation of **2** to the dearomatized complex **II**, which is the active species in the [1,3]-addition of CO₂. As mentioned previously, the reaction of **2** with CO₂ in THF is rapid at ambient temperature. THF, as a coordinative polar solvent, can stabilize the polar transition state involved in the migration of the proton from the benzylic position to the metal center to give complex **II**.

3. Conclusions

We have described the reversible binding of CO₂ to the dearomatized [(^tBuPNP*)Ir(COE)] (**1**) and to the aromatized [(^tBuPNP)Ir(C₆H₅)] (**2**) via metal-ligand cooperation. The reaction of the aromatized complex **2** with CO₂ is highly solvent dependent and takes place with THF at ambient temperature while in benzene heating at 80 °C is required. On the other hand, the already dearomatized **1** readily reacts with CO₂ both in THF or benzene at ambient temperature. Based on our observations we conclude that [1,3]-addition of CO₂ via MLC can take place only by dearomatized complexes or intermediates. In the case of **2**, formation of the hydrido phenyl dearomatized intermediate **II** is facilitated by the polar THF.

4. Experimental

4.1. General procedures

All experiments with metal complexes and phosphine ligands were carried out under a purified nitrogen atmosphere in a Vacuum Atmosphere glovebox equipped with an MO 40-2 inert gas purifier or using standard Schlenk techniques. All solvents were reagent grade or better. All non-deuterated solvents were refluxed over sodium/benzophenone ketyl and distilled under an argon atmosphere. Methylene chloride and acetone were used as received and dried over 4 Å molecular sieves and calcium sulfate, respectively. Complexes [(^tBuPNP*)Ir(COE)] (**1**) [22], [(^tBuPNP)Ir(C₆H₆)] (**2**) [22] and IrCl(DMSO)₄ [39] were prepared according to literature procedures. Deuterated solvents were used as received. All the solvents were degassed with argon and kept in the glove box over 4 Å molecular sieves (acetone was kept over calcium sulfate). Commercially available reagents were used as received. ¹H, ¹³C and ³¹P NMR spectra were recorded using a Bruker Avance III-300, Bruker Avance III-400 or Avance 500 NMR spectrometer. All spectra were recorded at 298 K unless otherwise indicated. ¹H NMR and ¹³C{¹H} NMR chemical shifts are reported in ppm downfield from tetramethylsilane. In ¹H NMR, the chemical shifts were referenced to the residual hydrogen signal of the deuterated solvents. In ¹³C{¹H} NMR measurements, the signals of deuterated solvents were used as a reference. ³¹P NMR chemical shifts are reported in parts per million downfield from H₃PO₄ and referenced to an external 85% solution of phosphoric acid in D₂O. Abbreviations used in the description of NMR data are as follows: br, broad; s, singlet; d, doublet; t, triplet; q, quartet; m, multiplet; v, virtual. Temperature calibration of the spectrometer was performed using CH₃OH/CD₃OD. IR spectra were recorded on Thermo Nicolet 6700 FT-IR.

4.2. Synthesis of [(^tBuPNP-COO)Ir(C₆H₅)(H)] (**7**)

To a THF-*d*₈ solution of [(^tBuPNP)Ir(C₆H₅)] (**2**) (10 mg, 0.015 mmol) in an NMR tube equipped with a septum was added CO₂ (1 ml, ~ 3 equiv) by a syringe. The color changed from grey-violet to light brown during 10 min. Complex **7** can be obtained also by addition of CO₂ to a preheated to 80 °C benzene solution of **2** (same concentration and CO₂ volume as mentioned above). The reaction in benzene was conducted in a J. Young NMR tube equipped with a septum. Complex **7** is unstable and under vacuum partially gives **2**, thus full NMR assignment of **7** was conducted *in-situ*. The NMR spectra of **7** are presented in the Supporting Information.

$^{31}\text{P}\{^1\text{H}\}$ NMR (THF- d_8): AB system centered at 56.75 ($^2J_{\text{PP}} = 356.3$ Hz) and 69.55 ($^2J_{\text{PP}} = 356.3$ Hz) ppm. ^1H NMR (500 MHz, THF- d_8) -24.07 (1H, dd, $^2J_{\text{PP}} = 18.8$, 7.5 Hz, Ir-*H*), appears as a singlet in $^1\text{H}\{^{31}\text{P}\}$, 1.03 (d, 9H, $^2J_{\text{PH}} = 12.1$ Hz, P-C(CH $_3$) $_3$), appears as a singlet in $^1\text{H}\{^{31}\text{P}\}$, 1.07 (d, 9H, $^2J_{\text{PH}} = 12.6$ Hz, P-C(CH $_3$) $_3$), appears as a singlet in $^1\text{H}\{^{31}\text{P}\}$, 1.18 (d, 9H, $^2J_{\text{PH}} = 12.8$ Hz, P-C(CH $_3$) $_3$), appears as a singlet in $^1\text{H}\{^{31}\text{P}\}$, 1.19 (d, 9H, $^2J_{\text{PH}} = 13.1$ Hz, P-C(CH $_3$) $_3$), appears as a singlet in $^1\text{H}\{^{31}\text{P}\}$, 3.30 (dd, 1H, $^2J_{\text{HH}} = 16.5$ Hz, $^2J_{\text{PH}} = 7.1$ Hz, P-CH $_2$ Py), appears as a doublet in $^1\text{H}\{^{31}\text{P}\}$, 3.94 (ddd, 1H, $^2J_{\text{HH}} = 16.5$ Hz, $^2J_{\text{PH}} = 9.9$ Hz, $^4J_{\text{PH}} = 2.4$ Hz, P-CH $_2$ Py), appears as a doublet in $^1\text{H}\{^{31}\text{P}\}$, 5.05 (dd, 1H, $^4J_{\text{PH}} = 2.5$ Hz, $^2J_{\text{PH}} = 6.4$ Hz, P-CHCOOPy appears as a singlet in $^1\text{H}\{^{31}\text{P}\}$, 6.57 (m, 1H, Aryl-H), 6.60 (dt, 1H, $^3J_{\text{HH}} = 7.1$ Hz, $^4J_{\text{HH}} = 1.8$ Hz, Aryl-H), 6.70 (dt, 1H, $^3J_{\text{HH}} = 7.1$ Hz, $^4J_{\text{HH}} = 1.8$ Hz, Aryl-H), 7.36 (d, 1H, $^3J_{\text{HH}} = 7.7$ Hz, Py-H), 7.49 (d, 1H, $^3J_{\text{HH}} = 8.0$ Hz, Py-H), 7.60 (d, 1H, $^3J_{\text{HH}} = 7.3$ Hz, Aryl-H), 7.76 (t, 1H, $^3J_{\text{HH}} = 7.7$ Hz, Py-H), 7.88 (d, 1H, $^3J_{\text{HH}} = 7.7$ Hz, Aryl-H). $^{13}\text{C}\{^1\text{H}\}$ NMR (THF- d_8): 29.20 – 30.4 (m, P-C(CH $_3$) $_3$), 34.73 (dd, $^3J_{\text{PC}} = 4.0$ Hz, $^1J_{\text{PC}} = 20.3$ Hz, P-C(CH $_3$) $_3$), 36.46 (dd, $^3J_{\text{PC}} = 3.9$ Hz, $^1J_{\text{PC}} = 13.7$ Hz, P-C(CH $_3$) $_3$), 38.58 (m, P-C(CH $_3$) $_3$), 39.19 (dd, $^3J_{\text{PC}} = 6.6$ Hz, $^1J_{\text{PC}} = 10.5$ Hz, P-C(CH $_3$) $_3$), 39.59 (d, $^1J_{\text{PC}} = 26.0$ Hz, CH $_2$ P), 65.16 (d, $^1J_{\text{PC}} = 11.7$ Hz, P-CHCOO-Py), 119.25 (d, $^3J_{\text{PC}} = 7.4$ Hz, Pyr-CH), 119.65 (d, $^3J_{\text{PC}} = 7.4$ Hz, Pyr-CH), 120.44 (s, Aryl-CH), 125.24 (s, Aryl-CH), 126.75 (s, Aryl-CH), 138.34 (s, Pyr-CH), 140.24 (s, Ary-CH), 148.67 (s, Aryl-CH), 132.6 (m, Cipso), 161.85 (s, Py-C), 162.97 (s, Py-C), 171.34 (dd, $^2J_{\text{PC}} = 7.8$ Hz, $^5J_{\text{PC}} = 2.2$ Hz, P-CHCOO-Py). IR($\nu(\text{COO-})$) = 1640 cm^{-1} . The structure was confirmed by DEPT, C-H correlation experiments (HMBC, HSQC) and 2D COSY NMR.

4.3. Synthesis of [(*t*BuPNP-COO)Ir(C $_8$ H $_{13}$)(H)] (**8**, **8'**)

To a benzene- d_6 solution of [(*t*BuPNP*)Ir(COE)] (**1**) (15 mg, 0.022 mmol) at 25 °C was added CO $_2$ in small excess (670 μL , ~ 0.03 mmol). The color changed from dark-red to orange during 10 min. Complexes **8** and **8'** were characterized *in situ*. The NMR spectra of the mixture of **8** and **8'** are presented in the Supporting Information.

8 + **8'**: $^{31}\text{P}\{^1\text{H}\}$ NMR (benzene- d_6): **8** AB system centered at 51.86 and 65.59 ppm (d, $^2J_{\text{PP}} = 368.4$ Hz), **8'** AB system centered at 57.42 and 62.77 (d, $^2J_{\text{PP}} = 374.5$ Hz). ^1H NMR (500 MHz, benzene- d_6) -25.16 (dd, 1H, $^2J_{\text{PH}} = 18.6$ Hz, $^2J_{\text{PH}} = 6.7$ Hz, appears as a singlet in $^1\text{H}\{^{31}\text{P}\}$, Ir-*H*), -24.98 (dd, 1H, $^2J_{\text{PH}} = 19.3$ Hz, $^2J_{\text{PH}} = 7.4$ Hz, appears as a singlet in $^1\text{H}\{^{31}\text{P}\}$, Ir-*H*), 0.75 (d, $^3J_{\text{PH}} = 11.9$ Hz, appears as a singlet in $^1\text{H}\{^{31}\text{P}\}$, P-C(CH $_3$) $_3$), 0.78 (d, $^3J_{\text{PH}} = 11.9$

Hz, appears as a singlet in $^1\text{H}\{^{31}\text{P}\}$, P-C(CH₃)₃, 0.87 (d, $^3J_{\text{PH}} = 12.4$ Hz, appears as a singlet in $^1\text{H}\{^{31}\text{P}\}$, P-C(CH₃)₃), 0.79 (d, $^3J_{\text{PH}} = 12.9$ Hz, appears as a singlet in $^1\text{H}\{^{31}\text{P}\}$, P-C(CH₃)₃), 1.06 (d, $^3J_{\text{PH}} = 10.3$ Hz, appears as a singlet in $^1\text{H}\{^{31}\text{P}\}$, P-C(CH₃)₃), 1.27 (d, $^3J_{\text{PH}} = 12.3$ Hz, appears as a singlet in $^1\text{H}\{^{31}\text{P}\}$, P-C(CH₃)₃), 1.29 (d, $^3J_{\text{PH}} = 12.3$ Hz, appears as a singlet in $^1\text{H}\{^{31}\text{P}\}$, P-C(CH₃)₃), 1.56 (d, $^3J_{\text{PH}} = 11.8$ Hz, appears as a singlet in $^1\text{H}\{^{31}\text{P}\}$, P-C(CH₃)₃), 1.60 (d, $^3J_{\text{PH}} = 12.3$ Hz, appears as a singlet in $^1\text{H}\{^{31}\text{P}\}$, P-C(CH₃)₃), 1.69 – 2.06 (m, CH₂-COE), 2.02 (m, Ir-C=CH-CH₂), 2.36 (m, Ir-C=CH-CH₂), 2.57 (m, Ir-C=CH-CH₂), 2.67 (m, Ir-C=CH-CH₂), 2.6 (m, P-CH₂Py), 2.84 (m, Ir-C=CH), 3.2 (m, P-CH₂Py), 3.27 (m, Ir-C=CH), 4.99 (dd, 1H, $^4J_{\text{PH}} = 2.1$ Hz, $^2J_{\text{PH}} = 6.1$ Hz, P-CHCOO-Py), 5.05 (dd, 1H, $^4J_{\text{PH}} = 2.1$ Hz, $^2J_{\text{PH}} = 6.3$ Hz, P-CHCOO-Py), 6.03 (t, 1H, $^3J_{\text{HH}} = 7.9$ Hz, Ir-C=C-H), 6.40 (t, 1H, $^3J_{\text{HH}} = 7.9$ Hz, Ir-C=C-H), 6.46 (d, 1H, $^3J_{\text{HH}} = 7.3$ Hz, Py-CH), 6.48 (d, 1H, $^3J_{\text{HH}} = 7.7$ Hz, Py-CH), 6.87 (d, 2H, $^3J_{\text{HH}} = 7.7$ Hz, Py-CH), 6.98 – 7.02 (m, 2H, Py-CH), $^{13}\text{C}\{^1\text{H}\}$ NMR (benzene-*d*₆): 27.2 – 32.2 (m, P-C(CH₃)₃, P-C(CH₃)₃, COE-CH₂), 40.34 (d, $^1J_{\text{PC}} = 24.6$ Hz, Py-CH₂-P), 51.67 (d, $^3J_{\text{PC}} = 6.4$ Hz, Ir-C-CH₂), 64.90 (d, $^2J_{\text{PC}} = 12.2$ Hz, P-CHCOO-Py), 65.1 (br d, $^2J_{\text{PC}} = 14$ Hz, P-CHCOO-Py), 118.20 (d, $^3J_{\text{PC}} = 6.0$ Hz, Py-CH), 118.36 (d, $^3J_{\text{PC}} = 5.4$ Hz, Py-CH), 118.20 (d, $^3J_{\text{PC}} = 6.0$ Hz, Py-CH), 120.49 (m, Py-CH), 24.7 (m, Ir-C=CH), 128.5 (m, Ir-C=CH), 130.3 (br s, Ir-C=CH), 136.73 (s, Py-CH), 136.82 (s, Py-CH), 137.08 (d, $^3J_{\text{PC}} = 5.4$ Hz, Ir-C=CH), 160.3 (br s, Py-C), 160.8 (br s, Py-C), 161.0 (br s, Py-C), 161.1 (br s, Py-C), 171.44 (dd, $^3J_{\text{PC}} = 2.2$ Hz, $^2J_{\text{PC}} = 7.0$ Hz, COO-Ir) and 171.86 ppm (dd, $^3J_{\text{PC}} = 2.3$ Hz, $^2J_{\text{PC}} = 8.2$ Hz, COO-Ir). IR $\nu_{\text{CO}}(\text{COO-}) = 1635$ cm⁻¹. The structure was confirmed by DEPT, C-H correlation experiments (HMBC, HSQC) and 2D COSY NMR.

4.4. CO₂/¹³CO₂ exchange in **7** and **8**, **8'**

To a THF solution of **7** or **8**, **8'** in an NMR tube equipped with septum, 1 equiv of ¹³CO₂ was added via a syringe. The exchange reaction was monitored by $^{13}\text{C}\{^1\text{H}\}$ NMR spectroscopy.

4.5. Synthesis of [(^tBuPNP)IrCl] (**10**)

A benzene solution of ^tBuPNP ligand (34.4 mg, 0.087 mmol) and [Ir(DMSO)₃Cl] (40.3 mg, 0.087 mmol) in a sealed thick-walled glass tube was heated at 65 °C for 3 h during which the color changed from yellow to purple. The solvent was removed under vacuum to give a brown solid. The solid was re-dissolved in pentane (5 ml) and toluene (1 ml) and was left at -20 °C for 2 days. The precipitate was isolated by decantation, washed with pentane (3×3 ml) and dried under

vacuum to give **10** as a brown-deep red solid in 83% yield. Crystals suitable for X-ray analysis were obtained from a pentane/toluene solution at -20 °C. Complex **10** is highly reactive towards O₂, and thus elemental analysis was not performed. The NMR spectra of **10** are presented in the Supporting Information.

³¹P{¹H} NMR (121 MHz, benzene-*d*₆): 49.87 (s). ¹H NMR (500 MHz, benzene-*d*₆): 1.46 (vt, 36H, *J*_{PH} = 6.5 Hz, P-C(CH₃)₃), 1.95 (vt, 4H, ²*J*_{PH} = 3.4 Hz, P-CH₂Py), 6.17 (d, 2H, ³*J*_{HH} = 7.6 Hz, Py-*H*), 7.71 (t, 1H, ³*J*_{HH} = 7.6 Hz, Py-*H*). ¹³C{¹H} NMR (126 MHz, benzene-*d*₆): 29.19 (vt, *J*_{PC} = 2.9 Hz, P-C(CH₃)₃), 35.51 (vt, *J*_{PC} = 9.7 Hz, P-C(CH₃)₃), 38.11 (vt, *J*_{PC} = 8.8 Hz, P-CH₂Py), 121.17 (vt, *J*_{PC} = 5.1 Hz, Py-CH), 124.31 (s, Py-CH), 164.06 (vt, *J*_{PC} = 5.5 Hz, Py-C).

4.6. Crystal structure determination

Data were collected at 100 K on either a Bruker APEX- II Kappa CCD for **10** or a dual source Rigaku XtaLab PRO diffractometer equipped with PILATUS 200 detector for **9**. Data were processed with SAINT or CrysAlisPRO, and structures were solved with SHELXS and SHELXT, respectively. Structures were further refined with full matrix least-squares based on F² with SHELXL. Hydrogens were calculated in riding mode. Hydride and the hydrogen on the carbonate were located in the electron density map. All crystallographic data are presented in table S1, Supporting Information.

Supplementary material

NMR spectra of **7**, **8** and **8'** and crystallographic data of **9** and **10** (PDF). Crystallographic data of **9** and **10** (CIF).

Acknowledgement

This manuscript is dedicated to Prof. Dan Meyerstein in recognition of his many important contributions to chemistry. This research was supported by the European Research Council (ERC AdG 692775). D.M. holds the Israel Matz Professorial Chair of Organic Chemistry.

References

- [1] J.R. Khusnutdinova, D. Milstein. *Angew. Chem. Int. Ed.*, **54**, 12236 (2015).
- [2] D. Milstein. *Trans. Philosoph. R. Soc. A*, **373**, 20140189 (2015).

- [3] T. Zell, D. Milstein. *Acc. Chem. Res.*, **48**, 1979 (2015).
- [4] C. Gunanathan, D. Milstein. *Acc. Chem. Res.*, **44**, 588 (2011).
- [5] C. Gunanathan, D. Milstein, Bond Activation by Metal-Ligand Cooperation: Design of “Green” Catalytic Reactions Based on Aromatization-De aromatization of Pincer Complexes, in: T. Ikariya, M. Shibasaki (Eds.), *Bifunctional Molecular Catalysis*, Springer (2011), pp. 55-84.
- [6] D. Milstein. *Top. Catal.*, **53**, 915 (2010).
- [7] M. Montag, J. Zhang, D. Milstein. *J. Am. Chem. Soc.*, **134**, 10325 (2012).
- [8] J. Zhang, G. Leituss, Y. Ben-David, D. Milstein. *J. Am. Chem. Soc.*, **127**, 10840 (2005).
- [9] C. Gunanathan, Y. Ben-David, D. Milstein. *Science*, **317**, 790 (2007).
- [10] E. Fogler, J.A. Garg, P. Hu, G. Leituss, L.J.W. Shimon, D. Milstein. *Chem. Eur. J.*, **20**, 15727 (2014).
- [11] P. Hu, Y. Diskin-Posner, Y. Ben-David, D. Milstein. *ACS Catal.*, **4**, 2649 (2014).
- [12] C. Gunanathan, B. Gnanaprakasam, M.A. Iron, L.J.W. Shimon, D. Milstein. *J. Am. Chem. Soc.*, **132**, 14763 (2010).
- [13] E. Balaraman, B. Gnanaprakasam, L.J.W. Shimon, D. Milstein. *J. Am. Chem. Soc.*, **132**, 16756 (2010).
- [14] M. Feller, Y. Diskin-Posner, L.J.W. Shimon, E. Ben-Ari, D. Milstein. *Organometallics*, **31**, 4083 (2012).
- [15] J.O. Bauer, G. Leituss, Y. Ben-David, D. Milstein. *ACS Catal.*, **6**, 8415 (2016).
- [16] M. Vogt, A. Nerush, M.A. Iron, G. Leituss, Y. Diskin-Posner, L.J.W. Shimon, Y. Ben-David, D. Milstein. *J. Am. Chem. Soc.*, **135**, 17004 (2013).
- [17] A. Nerush, M. Vogt, U. Gellrich, G. Leituss, Y. Ben-David, D. Milstein. *J. Am. Chem. Soc.*, **138**, 6985 (2016).
- [18] A. Anaby, B. Butschke, Y. Ben-David, L.J.W. Shimon, G. Leituss, M. Feller, D. Milstein. *Organometallics*, **33**, 3716 (2014).
- [19] J. Zhang, G. Leituss, Y. Ben-David, D. Milstein. *Angew. Chem. Int. Ed.*, **45**, 1113 (2006).
- [20] L. Schwartzburd, M.A. Iron, L. Konstantinovski, E. Ben-Ari, D. Milstein. *Organometallics*, **30**, 2721 (2011).
- [21] R. Langer, G. Leituss, Y. Ben-David, D. Milstein. *Angew. Chem., Int. Ed.*, **50**, 2120 (2011).

- [22] E. Ben-Ari, G. Leitus, L.J.W. Shimon, D. Milstein. *J. Am. Chem. Soc.*, **128**, 15390 (2006).
- [23] L. Schwartsburd, M.A. Iron, L. Konstantinovski, Y. Diskin-Posner, G. Leitus, L.J.W. Shimon, D. Milstein. *Organometallics*, **29**, 3817 (2010).
- [24] M. Vogt, M. Gargir, M.A. Iron, Y. Diskin-Posner, Y. Ben-David, D. Milstein. *Chem. Eur. J.*, **18**, 9194 (2012).
- [25] M. Vogt, O. Rivada-Whealaghan, M.A. Iron, G. Leitus, Y. Diskin-Posner, L.J.W. Shimon, Y. Ben-David, D. Milstein. *Organometallics*, **32**, 300 (2013).
- [26] C.A. Huff, J.W. Kampf, M.S. Sanford. *Organometallics*, **31**, 4643 (2012).
- [27] M. Feller, U. Gellrich, A. Anaby, Y. Diskin-Posner, D. Milstein. *J. Am. Chem. Soc.*, **138**, 6445 (2016).
- [28] M. Vogt, A. Nerush, Y. Diskin-Posner, Y. Ben-David, D. Milstein. *Chem. Sci.*, **5**, 2043 (2014).
- [29] M. Montag, J. Zhang, D. Milstein. *J. Am. Chem. Soc.*, **134**, 10325 (2012).
- [30] M. Vogt, A. Nerush, M.A. Iron, G. Leitus, Y. Diskin-Posner, L.J.W. Shimon, Y. Ben-David, D. Milstein. *J. Am. Chem. Soc.*, **135**, 17004 (2013).
- [31] M.A. Iron, E. Ben-Ari, R. Cohen, D. Milstein. *Dalton Trans.*, 9433 (2009).
- [32] M. Feller, E. Ben-Ari, Y. Diskin-Posner, R. Carmieli, L. Weiner, D. Milstein. *J. Am. Chem. Soc.*, **137**, 4634 (2015).
- [33] Q. Liu, L. Wu, R. Jackstell, M. Beller. *Nat. Comm.*, **6**, 5933 (2015).
- [34] E.V. Kondratenko, G. Mul, J. Baltrusaitis, G.O. Larrazabal, J. Perez-Ramirez. *Energy Environ. Sci.*, **6**, 3112 (2013).
- [35] M. Aresta, A. Dibenedetto, A. Angelini. *Chem. Rev.*, **114**, 1709 (2014).
- [36] J. Artz, T.E. Müller, K. Thenert, J. Kleinekorte, R. Meys, A. Sternberg, A. Bardow, W. Leitner. *Chem. Rev.*, **118**, 434 (2018).
- [37] M. Cokoja, C. Bruckmeier, B. Rieger, W.A. Herrmann, F.E. Kühn. *Angew. Chem. Int. Ed.*, **50**, 8510 (2011).
- [38] F.J. Fernández-Alvarez, M. Iglesias, L.A. Oro, V. Polo. *ChemCatChem*, **5**, 3481 (2013).
- [39] R. Dorta, H. Rozenberg, L.J.W. Shimon, D. Milstein. *Chem. Eur. J.*, **9**, 5237 (2003).

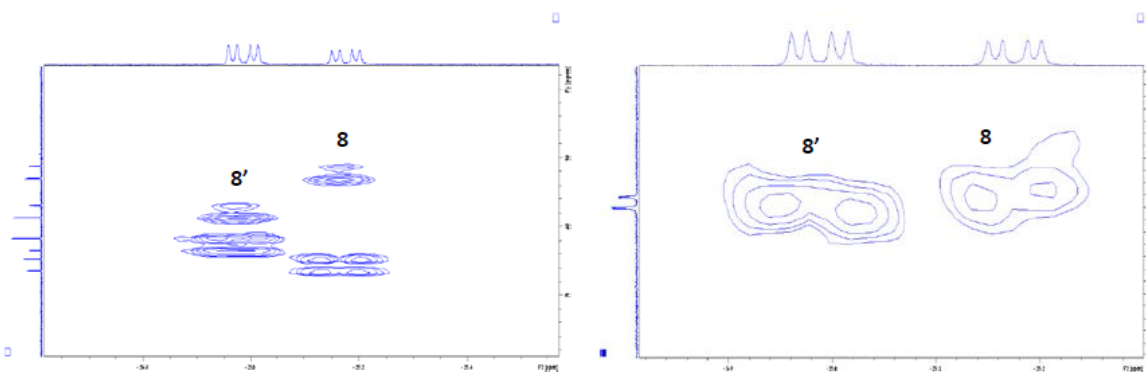


Figure 1. P-H correlation (left) and C-H long range correlation (HMBC) (right) 2D NMR experiments of **8** and **8'**.

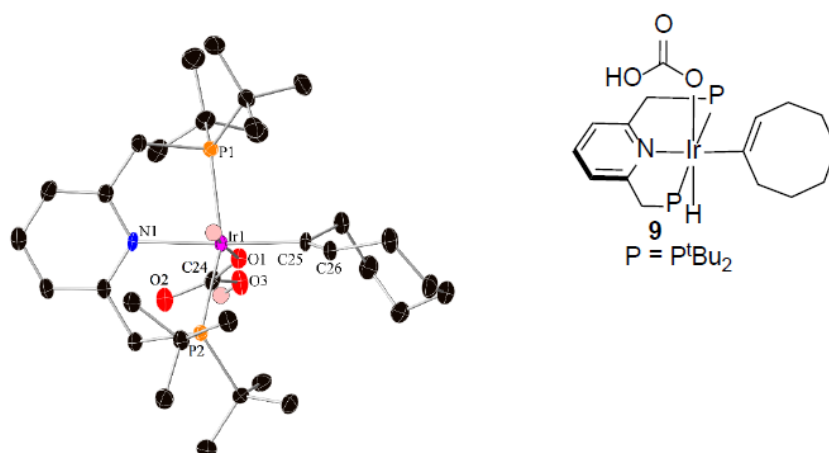


Figure 2. Crystal structure of **9**. Atoms are presented as thermal ellipsoids at 50% probability level. Hydrogens are omitted for clarity except the hydride and carbonate hydrogen, presented as small pink spheres. Selected bond lengths (Å) and angles (deg): Ir(1)–H(1) 1.38(4), Ir(1)–P(1) 2.3246(7), Ir(1)–P(2) 2.3125(7), Ir(1)–N(1) 2.168(2), Ir(1)–O(1) 2.210(2), Ir(1)–C(25) 2.088(3), C(24)–O(1) 1.249(4), C(24)–O(2) 1.257(4), C(24)–O(3) 1.355(4), C(25)–C(26) 1.344(4), C(25)–C(32) 1.513(4), P(1)–Ir(1)–P(2) 159.22(3), N(1)–Ir(1)–C(25) 176.34(10), H(1)–Ir(1)–O(1) 176.1(16).

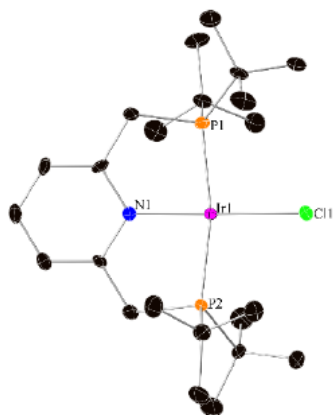


Figure 3. Crystal structure of **10**. Atoms presented as thermal ellipsoids at 50% probability level. Hydrogens are omitted for clarity. Selected bond lengths (Å) and angles (deg): Ir(1)–N(1) 2.007(6), Ir(1)–P(1) 2.268(2), Ir(1)–P(2) 2.251(17), Ir(1)–Cl(1) 2.361(2), P(1)–Ir(1)–P(2) 168.34(8), N(1)–Ir(1)–Cl(1) 178.28(19).

Graphical abstract

